Surface Science 629 (2014) 102–107

Contents lists available at ScienceDirect

Surface Science

journal homepage: www.elsevier.com/locate/susc

Chiral assemblies of nickel lysinate via the corrosive adsorption of (*S*)-lysine on Ni/Au{111}

K.E. Wilson, C.J. Baddeley *

EaStCHEM School of Chemistry, University of St Andrews, St Andrews, Fife KY16 9ST, UK

ARTICLE INFO

Available online 4 April 2014

Keywords:
Chirality
STM
Amino acid
Nickel
Gold
Bioinorganic

ABSTRACT

The adsorption of (*S*)-lysine onto submonolayer coverages of Ni on Au{111} was investigated by scanning tunnelling microscopy and reflection absorption infrared spectroscopy. Arrays of two-dimensional Ni nanoclusters were prepared on the Au{111} surface. The sticking probability of (*S*)-lysine was found to increase by an order of magnitude on Au surfaces templated by Ni compared to the clean Au surface. (*S*)-lysine corrodes Ni from the edges of clusters forming nickel lysinate complexes which self-assemble to form ordered molecular arrays. Below a threshold coverage, the Ni clusters are completely destroyed by (*S*)-lysine adsorption. Under these conditions, extensive restructuring of the Au steps is observed. The implications of our work for understanding the role of chiral modifiers in Ni catalysed enantioselective catalysis are discussed.

1. Introduction

Understanding the interaction of biological molecules such as amino acids with surfaces is of fundamental interest in areas such as the development of biosensors [1] and in the design of biocompatible materials [2]. In addition, as inexpensive, readily available chiral molecules, amino acids have attracted considerable interest as chiral modifiers in enantioselective catalysis. Ni catalysts modified by the adsorption of amino acids from solution have been shown to be effective catalysts for the enantioselective hydrogenation of β-ketoesters [3]. This class of reactions and the enantioselective hydrogenation of α-ketoesters over Pt [4] are two of the most extensively studied examples of heterogeneous enantioselective catalysts. In each case, the ability of the metal surface to allow the selective creation of one enantiomeric product is thought to be associated with the establishment of control over the adsorption geometry of the prochiral molecule such that one enantiotopic face of the reactant adsorbs on the surface in preference to the other allowing coadsorbed hydrogen atoms to attack the C═O bond from beneath the bond resulting in the formation of exclusively one type of chiral centre. On an achiral surface, the adsorption energy of each enantiotopic face will be identical, so hydrogenation yields a racemic mixture of products. It is widely believed that the adsorption of the chiral modifier provides a docking site for the pro-chiral reagent favouring the adsorption of one enantiotopic face [4]. McFadden et al. [5] demonstrated that high Miller index faces of face centred cubic (fcc) metals can often exist as two forms which are non-superimposable mirror images if kink sites are adjacent to steps with different lengths. A means of classifying such surfaces as *R* or *S* depending on the spatial configuration of the steps adjacent to kink sites was established [5]. For example, the step-kink atomic arrangements on an fcc{643}^{R} surface are the mirror image of those on the fcc {643}^{S} surface [5]. A number of studies have demonstrated differences in adsorption energy of two enantiomers on two mirror-equivalent chiral surfaces [6–8]. On a typical metal nanoparticle, in the absence of any chiral influence, a racemic mixture of chiral step kink arrangements would be anticipated on statistical grounds. However, if for instance, a chiral modifier selectively blocks one type of step-kink site or, more pertinent to this study, the chiral modifier reconstructs the surface metal atoms into a chiral arrangement, the step-kink sites could contribute significantly to the enantioselectivity of the catalyst. For example, we have shown that the modification conditions that produce the most enantioselective (*S*)-aspartic acid modified Ni catalyst [9], result in modifier coverages on the metal surface that are below detection limits of X-ray photoelectron spectroscopy (XPS) [10] and reflection absorption infrared spectroscopy (RAIRS) [11]. It has been proposed that extracted Ni amino acid complexes may give rise to enantioselective catalysis either on the surface of remaining Ni or even in solution [3]. We noted that as Ni catalysts are routinely washed after the modification step, the implication of having no remaining adsorbed aspartate species leads to the conclusion that residual chiral arrangements of Ni atoms contribute to the enantioselectivity of Ni-based catalysts [10,11].

In this study, we investigate the adsorption of (*S*)-lysine onto surfaces consisting of sub-monolayer coverages of Ni on Au{111}. We use scanning tunnelling microscopy (STM); RAIRS and temperature programmed desorption (TPD) to investigate the adsorption of (*S*)-lysine as functions of Ni coverage and adsorption temperature. As was originally demonstrated by Chambliss et al. [12], Ni nucleates into the elbows of the Au{111} herringbone reconstruction [13] giving nano-

* Corresponding author. Tel.: +44 1334 467236.
E-mail address: cjb14@st-and.ac.uk (C.J. Baddeley).

http://dx.doi.org/10.1016/j.susc.2014.03.026

sized two-dimensional (2D) clusters of Ni atoms. We have previously shown that the adsorption of (*S*)-glutamic acid causes the corrosion of Ni clusters and the formation of 1D chains of nickel pyroglutamate [14]. Zhao demonstrated that the adsorption of (*S*)-lysine onto the achiral Cu{001} surface resulted in the faceting of the surface such that {3 1 17}^{R} type facets were favoured over the mirror equivalent facets [15]. Recent studies by Gellman on {3 1 17}^{R} and {3 1 17}^{S} surfaces displayed an energetic preference for (*S*)-lysine adsorption on the {3 1 17}^{R} surface consistent with the earlier conclusions of Zhao [15]. In addition, we demonstrated that (*S*)-lysine can etch the Au{111} surface leading to the formation of Au nanofingers [16]. In this study, we show that adsorption of (*S*)-lysine onto Ni/Au{111} causes extensive etching of Ni and the formation of chiral assemblies of nickel (*S*)-lysinate complexes. The extent of etching is shown to be dependent on the initial size of Ni clusters. At low Ni coverage, etching completely destroys the Ni clusters and significant restructuring of Ni steps is observed.

2. Experimental details

Reflection absorption infrared spectroscopy (RAIRS) and scanning tunnelling microscopy (STM) experiments were conducted under ultra-high vacuum (UHV) conditions in an Omicron variable-temperature STM system with a base pressure of 1×10^{-10} mbar, which also has facilities for sample cleaning via argon ion bombardment and characterization via low-energy electron diffraction (LEED). A Nicolet Nexus 860 FTIR spectrometer was used to acquire RAIRS data (512 scans at a resolution of 4 cm^{-1}) using a mercury cadmium telluride (MCT) detector cooled by liquid nitrogen. The angles of incidence and reflection of the IR beam are each approximately 8° from the surface plane. A background spectrum of the Ni/Au{111} surface was taken prior to exposure to (*S*)-lysine ($NH_2 \cdot (CH_2)_4 \cdot NH_2CHCOOH$) (>98% Sigma). All STM experiments were acquired in constant-current mode using an electrochemically etched W tip. STM topographic images were processed using WSxM software [17]. In all experiments, the Au{111} sample was cleaned by cycles of ion sputtering (Ar^+, 0.9 kV, sample 8 μA) and annealing to 873 K until the LEED pattern characteristic of the Au{111}-($\sqrt{3} \times 22$) herringbone reconstruction was obtained [13]. Ni deposition was achieved by resistively heating a W filament around which a Ni wire had been wound. The Ni deposition rate was calibrated via STM by monitoring the size of the 2-D Ni clusters that nucleate into elbows of the herringbone reconstruction [12]. Ni coverages are reported in monolayers (ML) where 1 ML of Ni corresponds to one Ni atom for every surface Au atom. The prepared Ni/Au{111} surface was then exposed to (*S*)-lysine via sublimation from a solid doser. The temperature of lysine was monitored via a thermocouple and was maintained at 410 K for all experiments.

3. Results and discussion

3.1. Reflection absorption infrared spectroscopy (RAIRS)

Fig. 1a displays the RAIR spectra following the adsorption of (*S*)-lysine on 0.5 ML Ni on Au{111} at 300 K. Fig. 1b and c shows RAIRS data following analogous experiments on Au{111} and Ni{111}.

There are close similarities between the RAIR spectra acquired from Ni{111} and 0.5 ML Ni/Au{111} surfaces. By contrast, a similar lysine dose on Au{111} results in much weaker absorption bands and significant differences in the positions of the observed absorption bands. The sticking probability of lysine on Ni is an order of magnitude higher than on Au indicating that initial adsorption on the 0.5 ML Ni/Au{111} surface is dominated by adsorption on the Ni clusters.

On 0.5 ML Ni/Au{111} at low lysine exposure, bands are observed at 2933, 2871, 1643, 1616, 1578, 1469, 1414 and 1338 cm^{-1}. With increasing exposure, these bands increase in relative intensity and additional bands are observed at 3178, 1508, 1367, 1250, 1184 and 1157 cm^{-1}. The behaviour on Ni{111} is very similar. On Au{111}, fewer bands are observed with the main features at 2927, 2871, 1604 (a relatively broad feature) and 1396 cm^{-1}. Using previous investigations by Humblot et al. [18–20] and Stewart and Fredericks [21], band assignments are presented in Table 1. As is generally the case with FTIR studies of adsorbed amino acids, a key aim is to establish the charge state of the amino acid. The lack of a band in the 1700–1750 cm^{-1} range under any conditions signifies that the carboxylic acid functional group is deprotonated at all coverages and on all three surfaces. This is confirmed by the presence of bands which may be assigned to the symmetric (1395–1415 cm^{-1}) and asymmetric (1570–1580 cm^{-1}) stretches of the carboxylate functionality. At high lysine exposure, the RAIR spectra are rather similar to those presented by Humblot et al. following the adsorption of (*S*)-lysine onto Cu{110} [18]. On Ni{111} and on 0.5 ML Ni on Au{111}, the existence of a band in the 1640–1670 cm^{-1} range (δ_{as} (NH_3^+)) at low coverage is indicative of initial adsorption in the zwitterionic form as has been observed following amino acid adsorption on Ni [22] and Pd [23] surfaces. As the coverage is increased, these bands become relatively less intense compared to the δ_{asym} (NH_2) which appears in the 1605–1620 cm^{-1} range. Since (*S*)-lysine contains two amine functionalities, the increase in relative intensity of the δ_{asym} (NH_2) band may be associated with a reorientation of the terminal amine group while the zwitterionic form of the amino acid is retained through to the multilayer. By application of the metal surface dipole selection rule, the fact that the symmetric and asymmetric OCO stretching modes are each observed as relatively intense bands implies that the two O atoms of the carboxylate are not equidistant from the surface — i.e. in contrast to the most common adsorption geometry of amino acids on metal surfaces such as copper [24]. The band at 3178 cm^{-1} is characteristic of amino acids involved in H-bonding interactions usually following multilayer growth at 300 K [18]. The appearance of this band at ~600–900 s for (*S*)-lysine adsorption on Ni{111} is indicative that this exposure time corresponds to the onset of multilayer formation.

The fact that the interaction of lysine with Au is relatively weak leads to intermolecular interactions dominating the ordering process [16]. This is likely to force the carboxylate group to be close to planar to the surface which, by application of the surface dipole selection rule, would be an additional factor accounting for the relatively weak intensity of absorption bands.

3.2. Scanning tunnelling microscopy (STM)

3.2.1. (S)-lysine on 0.5 ML Ni/Au{111}

Fig. 2b–d shows STM images after a 0.50 ± 0.05 ML Ni on Au{111} surface (Fig. 2a) is exposed to a 30 s dose of (*S*)-lysine at 300 K. Analysis of cluster sizes and the overall area occupied by the clusters reveals that, after exposure to lysine, the cluster area decreased to 0.32 ± 0.05 ML and the cluster shapes are strongly corroded in comparison to the typical hexagonal shape of the as-deposited metallic clusters [12]. Molecular species are observed both between and on top of the residual Ni clusters (Fig. 2b–c). On top of the clusters, the molecular features exhibit no clear long range order. In contrast, the regions between the Ni clusters are covered in highly ordered arrays of molecular features (Fig. 2c–d). Under similar (*S*)-lysine dosing conditions, extensive arrays of ordered molecular features are not observed on Au{111} [16]. On Au{111}, when imaging at 300 K, small islands of ordered molecular arrangements are observed but the vast majority of the surface contains no evidence of self-assembled arrays [16]. The change in Ni cluster size coupled with the creation of densely packed molecular islands provides a strong indication that (*S*)-lysine has etched some Ni from the metallic particles to create lysine coordinated Ni species which are able to disperse across the surface and self-assemble into ordered arrangements. The formation of metal organic species at surfaces via analogous processes has been widely reported [25,26]. For example, metal organic coordination networks on surfaces have been identified based on the interaction of metal ions with carboxylates [27,28], nitriles [29], isocyanides [30,31] and imides [32,33].

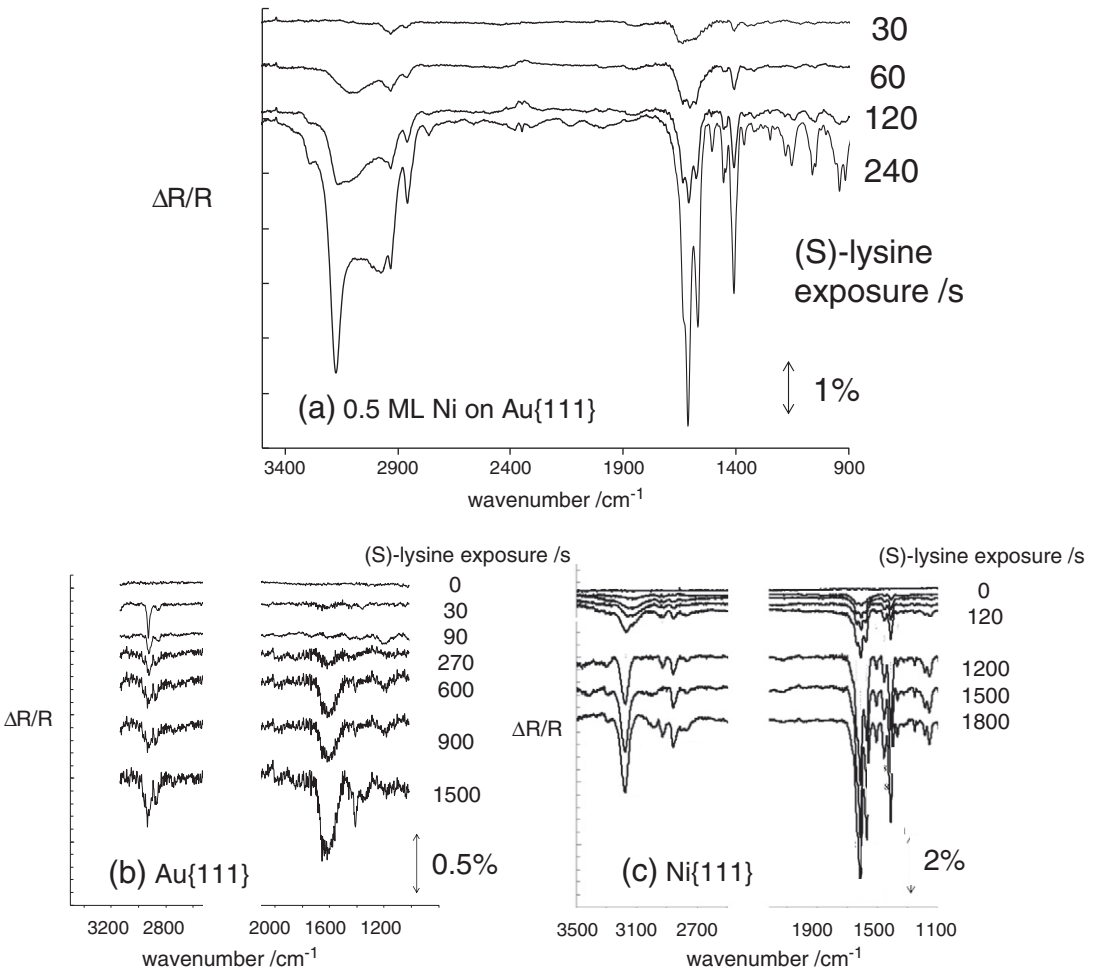

Fig. 1. RAIR spectra as a function of increasing time of (*S*)-lysine exposure at 300 K. (a) 0.5 ML Ni on Au{111}; (b) Au{111} and (c) Ni{111}.

At 300 K, the most common structure exhibits a pseudo-hexagonal arrangement of molecular features. One direction of molecular alignment has a repeat spacing of 8.9 Å at an angle of ~135° to the $[11\bar{2}]$ direction (Fig. 2d). Molecules are also aligned with a spacing of 7.6 Å with an angle between the two directions of ~120°. These dimensions are consistent with a commensurate unit cell of $<7\ -2\ |\ 1\ 2>$ as shown in Fig. 2f. This unit cell has dimensions of 18.0 Å × 7.6 Å suggesting that the long dimension of the unit cell contains two molecular features in inequivalent sites. We have no direct evidence (for example from low energy electron diffraction) that a commensurate overlayer has been formed. However, the identification of well-defined rotational domains suggests that the growth directions of the molecular domains are strongly influenced by the substrate. Hence we searched for commensurate unit cells that were consistent (within the error margin associated with thermal drift etc.) with the dimensions and directions of the molecular features observed by STM. For an achiral adsorbate, one would expect to observe reflectionally equivalent domains. However, the chirality of the (*S*)-lysine adsorbate would lead to different

Table 1
Assignments of RAIRS bands of (*S*)-lysine on 0.5 ML Ni on Au{111} following adsorption of lysine at 300 K. Bands are compared with data acquired on Au{111} and Ni{111}.

(*S*)-lysine on Ni{111}		(*S*)-lysine on Au{111}		(*S*)-lysine on 0.5 ML Ni on Au{111}		Assignment
Low coverage	Multilayer	Low coverage	High coverage	Low coverage	Multilayer	
3183	3183			–	3178	ν (N–H)
2960	2931	2927	2927	2933	2931	ν_{as} (CH_2)
2858	2859	2869	2871	2871	2862	ν_s (CH_2)
						ν_{acid} C═O
1662	1662	–		1643	–	δ_{as} (NH_3^+)
1608	1608	1604	1604	1616	1616	δ (NH_2)
–	1574			1578	1571	ν_{as} (COO^-)
–	1508			–	1508	δ_s (NH_3^+)
1460	1458	1448	1458	1469	1458	δ (CH_2)
1415	1411	–	1396	1414	1412	ν_s (COO^-)
–	1369	–	–		1367	CH_2 symmetric bend
1335, 1313	1340, 1311			1338	1336	CH_2 wag
–	1252	1265	1268	–	1250	ν (C–O) + δ (O–H)
1151	1186, 1157	1189	1182	–	1184, 1157	NH_2 wag
		1120	1124			ν (CN)

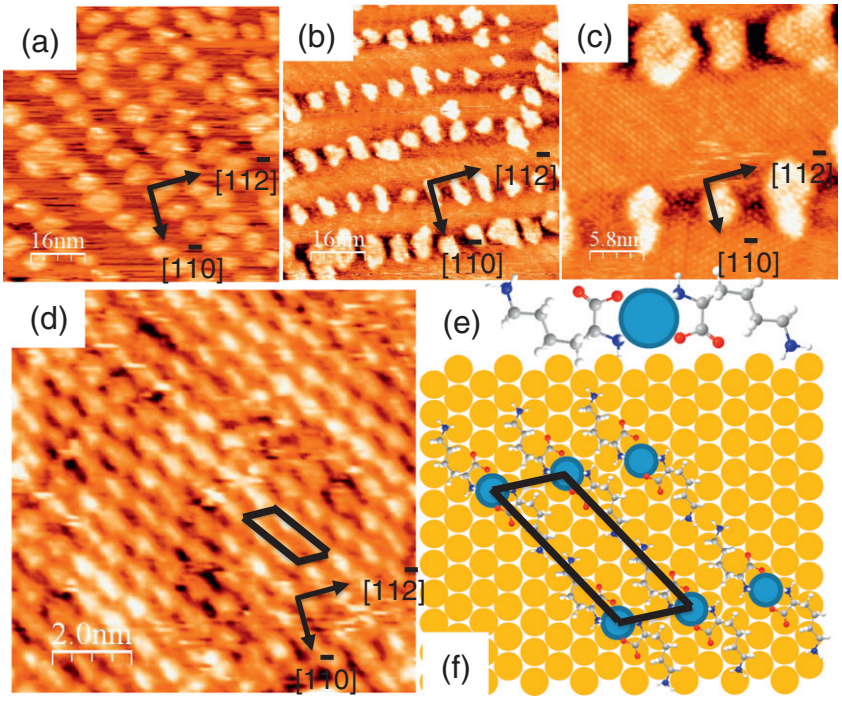

Fig. 2. STM images illustrating a) 0.5 ML Ni on Au{111} (80 nm × 80 nm, −1.0 V, 0.5 nA) b) 0.5 ML Ni on Au{111} after adsorption of (*S*)-lysine at 300 K (80 nm × 80 nm, 0.9 V, 1.2 nA); c) (29.0 nm × 29.0 nm, −1 V, 0.5 nA); d) (10 × 10 nm, 0.9 V, 1.2 nA); e) proposed arrangement of Ni(lysinate)$_2$ complexes; f) model for the surface arrangement of Ni(lysinate)$_2$ complexes.

intermolecular interactions if the adsorbate were forced to adopt the mirror equivalent arrangement. We were unable to find examples of reflectionally equivalent unit cells. Interestingly, we found a strong tendency in a given domain of the herringbone reconstruction for a single rotational domain of the ordered structure to be identified while in the adjacent region of the herringbone reconstruction a different rotational domain was observed. The herringbone reconstruction was found to have a similar influence on the growth directions of 1D chains of nickel pyroglutamate on Au{111} [34]. The unit cell is similar in dimensions to, but distinguishable from that observed in small islands of order for lysine on Au{111} [16]. In the lysine/Au case a unit cell was identified giving a <5 0 | 1 3> structure [16]. In the lysine/Ni/Au{111} case, the coverage of molecular features is 2 molecules per 16 Au atoms ($\theta = 0.125$ ML) compared to a coverage of 2 molecules for every 15 Au atoms ($\theta = 0.133$ ML) in the lysine/Au system [16]. Bearing in mind the decrease in Ni cluster area following lysine adsorption, we conclude that the structure observed consists of self-assembled Ni(lysinate)$_2$ species (Fig. 2e). The amount of extracted Ni included in the ordered arrays would be 0.063 ML. The quantity of Ni contained within these structures is of a similar order to the amount of Ni etched from the Ni clusters in the initial adsorption process. The propensity of lysine to etch Ni has been previously observed in an infrared study of lysine adsorbed onto several transition metal cation-substituted montmorillonites, including Ni [35]. Do Jang and Condrate concluded that two lysinate species co-ordinated to a Ni^{2+} ion via the N and one O atom of the amino acid functionalities forming a square planar complex but were unable to distinguish the absolute configuration of the N and O atoms around the central ion [35]. In our case, the presence of the surface allows us to conclude that the N atoms are positioned on opposite sides of the Ni ion in order to ensure that the C–H bond of the chiral centre points towards the surface. As shown in Fig. 2f, the ordered structure can be explained by the stacking of such complexes. The driving force for this particular structure seems to be the ability to form N–H—N hydrogen bonds between the terminal amine groups of adjacent complexes. The functional groups in the proposed structure are close to parallel to the Au{111} surface and so, by the application of the metal-surface dipole selection rule, one would expect weak intensities of bands associated with the vibrational modes of these groups. The RAIR spectrum would be dominated by the adsorption of lysine on the residual Ni clusters and would be expected to resemble the spectrum of lysine on Ni{111} — as is observed (Fig. 1).

At room temperature, small islands of a second ordered structure were observed. Following annealing to 350 K, this structure became significantly more widespread on the surface suggesting that its formation may be thermodynamically favoured but kinetically restricted (Fig. 3a). A unit cell containing 4 molecular features can be identified (Fig. 3b). The unit cell possesses a hexagonal structure with unit vectors of dimension 15.3 Å consistent with a commensurate <6 −2 | 2 4> arrangement. Each unit cell contains 28 Au atoms giving a molecular coverage of $\theta = 0.14$ ML. As with the <7 −2 | 1 2> structure, we conclude that the fundamental building block is a Ni(lysinate)$_2$ species such that each unit cell contains two side by side complexes giving rise to the four molecular features. The <6 −2 | 2 4> structure possesses a slightly higher density than the <7 −2 | 1 2> structure. The slightly compressed unit cell no longer allows an N–H—N hydrogen bond between the terminal NH_2 groups with the alkyl chain parallel to the surface (Fig. 3c). We conclude that the alkyl chains and their terminal NH_2 groups are likely to be rotated out of the surface plane in the <6 −2 | 2 4> structure (Fig. 3d). This reorientation could be the reason for the relative increase in intensity of the δ_{asym} (NH_2) band in the RAIR spectrum with increasing lysine coverage. The apparent pairing of adjacent complexes may be caused by intermolecular interactions involving the NH_2 groups. This intramolecular transformation may be kinetically limited and explain why the structure is not observed widely at 300 K. We considered the possibility that the increase in molecular density could be explained by (*S*)-lysine undergoing a thermally induced internal cyclisation to a cyclic lactam. We reported the thermally induced transformation from glutamate to pyroglutamate in the analogous study of glutamic acid on Ni/Au{111} [14]. The thermal condensation of lysine has been found not to follow a typical peptide preparation pathway; instead the N-terminus is blocked by the formation of a cyclic lactam and acylated ε-NH_2 group [36,37]. It was found that, in an aqueous solution and at a temperature between 150 and 170 °C, the formation of α-amino-ε-caprolactam was greatly favoured, with evolution of water [36]. The

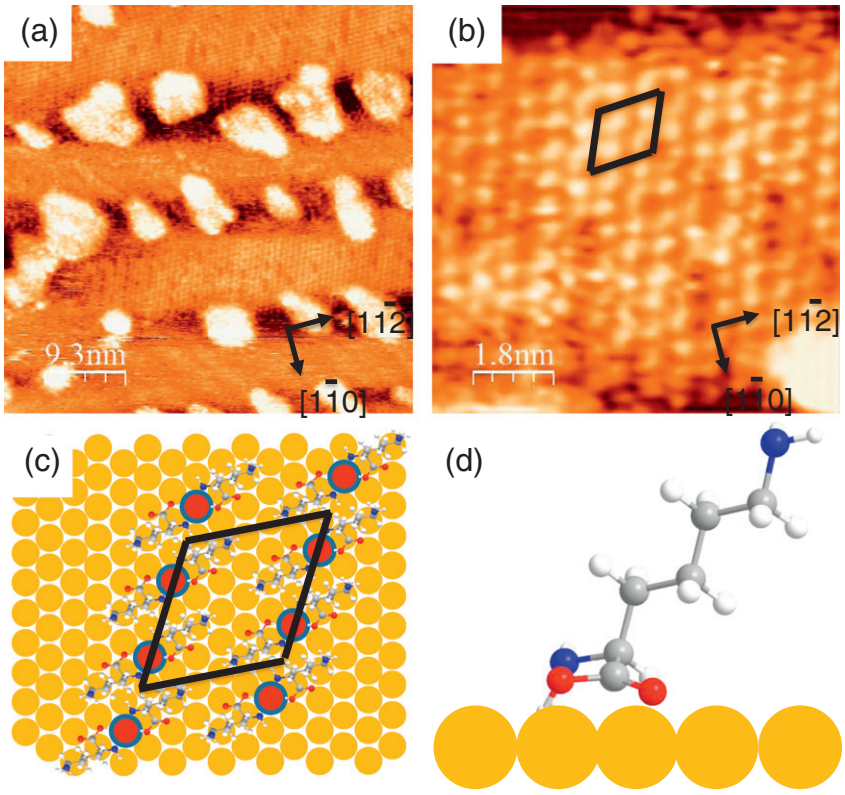

Fig. 3. STM images illustrating a) 0.5 ML Ni on Au{111} after adsorption of (*S*)-lysine at 300 K and annealing to 350 K (46.5 nm × 46.5 nm, 0.9 V, 2.2 nA); b) (9.0 × 9.0 nm, 0.9 V, 2.2 nA); c) model for the surface arrangement of Ni(lysinate)$_2$ complexes (d) side on view of the proposed adsorption geometry of the lysinate species in the STM images of Fig. 3a–b.

stability of a 7-membered lactam ring is well known, especially as the nitrogen atom within the ring is able to provide an empty π-orbital to allow aromatic stabilisation. It is possible that, with gentle heating to 350 K as carried out in the present experiment, the condensation of lysine species on top and at the edge of the Ni islands is catalysed by the metal, under UHV conditions, to form α-amino-ε-caprolactam. Vibrational spectroscopy at elevated temperatures would help to verify if such a process was occurring. Unfortunately, we are unable to carry out temperature dependent RAIRS experiments on our system.

After annealing to 380 K, no molecular structures could be detected between the residual Ni clusters. Our TPD measurements (supplementary information; Fig. S1) indicate that multilayers desorb at just above room temperature from the Ni/Au surface. This is consistent with the study by Cheong and Gellman of (*S*)-lysine on Cu{100}, where multilayer desorption is initiated at just above 300 K [38]. Decomposition/desorption of the Ni(lysinate)$_2$ complexes occurs by 380 K and a further decomposition and desorption of lysine (presumably from the Ni clusters) occurs at ~450 K.

3.3. (S)-lysine on 0.1 ML Ni/Au{111}

Fig. 4a shows an STM image of 0.10 ± 0.05 ML Ni/Au{111} surface which displays the characteristic growth of two-dimensional Ni clusters at the elbows of the Au{111} herringbone reconstruction [12]. Fig. 4b shows an STM image of the same surface following exposure to 1800 s (*S*)-lysine at 300 K. It is immediately apparent that neither Ni clusters nor any direct evidence of molecular ordering is observed. The step-edges of the Au{111} surface have undergone restructuring in a similar manner to that observed following lysine adsorption on Au{111} [16]. The disappearance of the Ni clusters mirrors the behaviour observed following the adsorption of glutamic acid onto Ni/Au{111} by Trant et al. [14] when it was reported that the corroded Ni became locked into

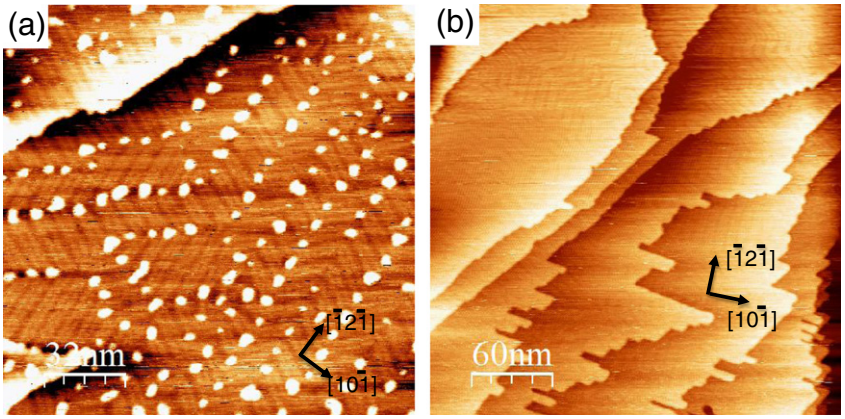

Fig. 4. STM images illustrating ~0.1 ML Ni on Au{111} (a) before (160 nm × 160 nm; −1 V, 2.0 nA) and (b) after (300 nm × 300 nm; −1 V, 1.0 nA) exposure to 1800 s (*S*)-lysine at 300 K.

one-dimensional chains consisting of amino acid complexes of nickel [14]. No evidence was found for the formation of any complexes or ordered molecular arrangements under these conditions. This lends further support to the fact that the self-assembled structures contain Ni. The surface coverage of lysine is limited by the amount of nickel which can be corroded from the clusters. If insufficient nickel is present, the ultimate coverage of nickel lysinate is not sufficient to saturate the monolayer and the complexes produced are presumably too mobile to be imaged at 300 K.

Despite no ordered molecular arrays being identified under these conditions, considerable evidence was found for the restructuring of the Au surface induced by (*S*)-lysine adsorption. In particular nanofingers were observed to grow away from the step edges and onto the Au terraces. The growth direction of the long dimension of the nanofingers makes an angle of ~10° with the $[10\bar{1}]$ direction of the Au surface (Fig. 2b). This direction is approximately consistent with the (7, −2) vector of the ordered structures shown in Fig. 2b, which makes an angle of 16° with the $[10\bar{1}]$ direction. It is well established that the facet directions induced by molecular adsorption tends to be determined by optimising interactions between step atoms and the molecular species [15,38,39]. In the present study it would make sense for nanofinger growth at 300 K to be related to the orientation of nickel lysinate species that is dominant at 300 K as was found to be the case when similar nanofingers were observed following lysine adsorption on Au{111} [16].

The mechanism of formation of self-assembled arrays of nickel lysinate is as follows. Initial adsorption occurs on the Ni clusters. Atoms at the edges of Ni clusters are easily oxidised and removed from the clusters by lysine. However, adsorption of lysine on the centre of Ni clusters stabilises the clusters such that there exists a threshold cluster size above which the cluster survives the etching process albeit reduced in size. Nickel lysinate complexes are able to self-assemble into two ordered arrangements. One arrangement (<7 −2 | 1 2>) is stabilised by intermolecular H-bonding between the terminal amine groups in an essentially flat lying geometry. The second arrangement (<6 −2 | 2 4>) is formed at elevated temperatures. This structure has a higher molecular density and is believed to form at higher temperatures via the reorientation of the aliphatic backbone of lysine to reduce the surface footprint. At low Ni coverages, clusters are completely destroyed. The lack of ordered structures observed under these conditions is likely to be associated with the inability to lock nickel lysinate complexes into two dimensional arrays owing to their high diffusion rates. Rearrangement of step atoms into chiral nanofingers is facilitated by the molecular species. It is likely that the direction of nanofinger growth is closely associated with the preferred surface orientation of nickel lysinate complexes.

The ability to 'spill over' nickel lysinate species onto Au surfaces with a high degree of control over the supramolecular assembly has potential to be adapted in bimetallic catalytic systems. Long range order of chiral modifiers has the potential to supply unique active sites for reactant molecules. Disordered, dense structures of amino acids on metal surfaces are less desirable as they fail to supply reactant molecules with uniform active sites. The heterogeneity of active sites available at solid surfaces has long been blamed for the lack of control over heterogeneous enantioselective processes.

4. Conclusions

The templating of a Au{111} surface with 2D nanoclusters of nickel causes an order of magnitude increase in the sticking probability of (*S*)-lysine at 300 K. For clusters containing a high ratio of edge to centre atoms, lysine is able to completely destroy the Ni clusters presumably via the oxidation of Ni atoms at the edges of clusters. Ni clusters with larger diameters become smaller, but survive the etching process due to becoming covered in chemisorbed zwitterionic lysine. In between the residual clusters, molecular features are observed to self-assemble into globally chiral <7 −2| 1 2> islands at 300 K and a more dense arrangement <6 −2| 2 4> at 350 K. These ordered arrays are constructed from self-assembled nickel (*S*)-lysinate complexes. We conclude that the higher density structure is formed via the reorientation of the aliphatic backbone of lysine to decrease the surface footprint of the metal organic complex. The nickel lysinate species decompose and/or desorb by 380 K. Adsorption of (*S*)-lysine onto Ni/Au{111} causes extensive etching of Ni. At low Ni coverages, where complete destruction of clusters is observed, no long range molecular ordering is observed at 300 K presumably due to the high mobility of the complexes at this temperature. Restructuring of steps results in the formation of nanofingers whose growth directions are chiral and are believed to be determined by the preferred orientation of nickel lysinate species on the Au surface.

Supplementary data to this article can be found online at http://dx.doi.org/10.1016/j.susc.2014.03.026.

Acknowledgements

KEW acknowledges the Engineering and Physical Sciences Research Council (EPSRC) for the award of a PhD studentship. We gratefully acknowledge Professor Neville Richardson for access to his UHV STM/RAIRS facility.

References

[1] B. Kasemo, Curr. Opinion Solid State Mater. Sci. 3 (1998) 451.
[2] J.C. Love, L.A. Estroff, J.K. Kriebel, R.G. Nuzzo, G.M. Whitesides, Chem. Rev. 105 (2005) 1103.
[3] Y. Izumi, Adv. Catal. 32 (1983) 215.
[4] A. Baiker, Catal. Today 100 (2005) 159.
[5] C.F. McFadden, P.S. Cremer, A.J. Gellman, Langmuir 12 (1996) 2483.
[6] B. Bhatia, D.S. Sholl, Angew. Chem. Int. Ed. 44 (2005) 7761.
[7] B. Bhatia, D.S. Sholl, J. Chem. Phys. 128 (2008) 144709.
[8] A.J. Gellman, J. Horvath, D.S. Sholl, T. Power, Abstr. Pap. Am. Chem. Soc. 219 (2000) 164 (PHYS).
[9] Y. Izumi, M. Imaida, H. Fukuwa, S. Akabori, Bull. Chem. Soc. Jpn. 42 (1963) 2373.
[10] K.E. Wilson, C.J. Baddeley, J. Catal. 278 (2011) 41.
[11] K.E. Wilson, C.J. Baddeley, J. Phys. Chem. C 113 (2009) 10706.
[12] D.D. Chambliss, R.J. Wilson, S. Chiang, Phys. Rev. Lett. 66 (1991) 1721.
[13] J.V. Barth, H. Brune, G. Ertl, R.J. Behm, Phys. Rev. B 42 (1990) 9307.
[14] A.G. Trant, T.E. Jones, C.J. Baddeley, J. Phys. Chem. C 111 (2007) 10534.
[15] X.Y. Zhao, J. Am. Chem. Soc. 122 (2000) 12584.
[16] K.E. Wilson, H.A. Früchtl, F. Grillo, C.J. Baddeley, Chem. Commun. 47 (2011) 10365.
[17] I. Horcas, R. Fernandez, J.M. Gomez-Rodriguez, J. Colchero, J. Gomez-Herrero, A.M. Baro, Rev. Sci. Instrum. 78 (2007) 013705.
[18] V. Humblot, C. Methivier, C.M. Pradier, Langmuir 22 (2006) 3089.
[19] V. Humblot, C. Methivier, R. Raval, C.M. Pradier, Surf. Sci. 601 (2007) 4189.
[20] F. Tielens, V. Humblot, C.M. Pradier, Surf. Sci. 602 (2008) 1032.
[21] S. Stewart, P.M. Fredericks, Spectrochim. Acta A Mol. Biomol. Spectrosc. 55 (1999) 1641.
[22] T.E. Jones, M.E. Urquhart, C.J. Baddeley, Surf. Sci. 587 (2005) 69.
[23] F. Gao, Y.L. Wang, L. Burkholder, W.T. Tysoe, Surf. Sci. 601 (2007) 3579.
[24] S.M. Barlow, R. Raval, Surf. Sci. Rep. 50 (2003) 201.
[25] L. Bartels, Nat. Chem. 2 (2010) 87.
[26] S. Stepanow, N. Lin, D. Payer, U. Schlickum, F. Klappenberger, G. Zoppellaro, M. Ruben, H. Brune, J.V. Barth, K. Kern, Angew. Chem. Int. Ed. 46 (2007) 710.
[27] M.A. Lingenfelder, H. Spillmann, A. Dmitriev, S. Stepanow, N. Lin, J.V. Barth, K. Kern, Chem. Eur. J. 10 (2004) 1913.
[28] S. Stepanow, N. Lin, F. Vidal, A. Landa, M. Ruben, J.V. Barth, K. Kern, Nano Lett. 5 (2005) 901.
[29] M. Luo, et al., J. Chem. Phys. 135 (2011) 134705.
[30] J. Boscoboinik, J. Kestell, M. Garvey, M. Weinert, W.T. Tysoe, Top. Catal. 54 (2011) 20.
[31] J.A. Boscoboinik, F.C. Calaza, Z. Habeeb, D.W. Bennett, D.J. Stacchiola, M.A. Purino, W.T. Tysoe, Phys. Chem. Chem. Phys. 12 (2010) 11624.
[32] S. Jensen, C.J. Baddeley, J. Phys. Chem. C 112 (2008) 15439.
[33] M. Yu, et al., Nano Res. 5 (2012) 903.
[34] A.G. Trant, C.J. Baddeley, Langmuir 27 (2011) 1788.
[35] S. Do Jang, R. Condrate, Clays Clay Miner. 20 (1972) 79.
[36] K. Harada, Bull. Chem. Soc. Jpn. 32 (1959) 1007.
[37] P. Melius, J. Yon-Ping Sheng, Bioorg. Chem. 4 (1975) 385.
[38] W.Y. Cheong, A.J. Gellman, J. Phys. Chem. C 115 (2011) 1031.
[39] Q. Chen, N.V. Richardson, Prog. Surf. Sci. 73 (2003) 59.